Nanoscale

ROYAL SOCIETY OF CHEMISTRY

COMMUNICATION

View Article Online
View Journal | View Issue



Cite this: *Nanoscale*, 2020, **12**, 22495

Received 10th June 2020,
Accepted 22nd October 2020

DOI: 10.1039/d0nr04415f

rsc.li/nanoscale

# Supramolecular nanomotors with "pH taxis" for active drug delivery in the tumor microenvironment†

Motilal Mathesh, Jiawei Sun, Frans van der Sandt and Daniela A. Wilson *



**Self-propelled nanomotors demonstrating autonomous motion in biologically relevant fuel are currently being studied to overcome the use of external physical or chemical stimuli as precise delivery agents. In this context, the tumor microenvironment (TME) with slightly acidic pH is used for developing cargo-releasing artificial systems triggered by such conditions. However, there is still a need for fabrication of smart nanomotors that can sense the acidic pH prevalent in the TME rather than using an external fuel source for selective activation and thereafter migrating towards tumors for active drug delivery. Herein, supramolecular assembly-based nanomotors are fabricated by *in-situ* grown $CaCO_3$ nanoparticles and studied for their motility behaviour in endogenously generated acidic pH by HeLa cells and further exploited as an active delivery vehicle for DOX molecules to the cells for their anticancer efficacy. The nanomotors are activated in slightly acidic pH showcasing "pH taxis" towards tumor cells without the need for any sophisticated/complicated technologies or an external fuel source for active and targeted delivery of drugs.**

## Introduction

Advancements in the field of artificial micro/nanomotors have shifted the niche of drug delivery systems (DDS) from passive to active autonomous systems. These active systems overcome the drawbacks of a passive delivery system that relies on passive accumulation in the target site, thus reducing the efficacy and bioavailability and increasing the associated high systemic toxicity. Active synthetic micro/nanomotors are also sought after due to their attractive capabilities in the field of biomedicine[1] such as biosensing,[2] cargo delivery[3] and nanosurgery[4] and can be actuated and controlled by an external source such as magnetic,[5–7] electric,[8,9] light[10–13] and ultrasound (US) acoustic wave sources.[14–17] With these advancements, researchers have fabricated artificial systems utilizing more than one chemical or physical stimuli for actuation for *in-vivo* studies and biomedical applications. For instance, our group has recently fabricated bowl-shaped stomatocyte nanomotors loaded with platinum/nickel (Pt/Ni) nanoparticles for propelled motion and enhanced directionality. Pt nanoparticles decomposed $H_2O_2$ to produce $O_2$ for propulsion, and the directionality was achieved by an external magnet in the presence of magnetic Ni nanoparticles.[6] In terms of biomedical applications, Pt-loaded stomatocytes were observed to show chemotactic behavior towards $H_2O_2$ produced by neutrophil cells.[18] Furthermore, once the Pt-loaded stomatocytes were fabricated by mixing PEG-*b*-PS and PEG-*b*-PCL, they were observed to degrade at acidic pH owing to the biodegradability of PCL and deliver doxorubicin (DOX) to cancer cells.[19] Other groups fabricated US-powered nanowire motors comprising nanoporous gold structures incorporated with DOX, where the drug release was triggered by near-infrared light due to photothermal effects.[20] Even though such systems have been studied extensively for biomedical applications, the use of a non-biocompatible fuel/external power source for guidance is not appropriate in a biological environment and has drawbacks in terms of delicate manipulation and requires specialists and sophisticated equipment.[21] In order to circumvent this problem, designing artificial systems powered by fuels inherently present in the body fluids or their constituents would be beneficial.[22]

Recently, fabrication of nanoconstructs for active delivery of drugs by using the *in-vivo* conditions of the tumor microenvironment (TME) is being studied. The most commonly used active DDS for tumor cells are based on the difference in redox states, pH and biomolecules between tumor cells and healthy cells.[23] Herein, we focus on slightly acidic conditions observed in tumor cells that have been utilized for powering mico/nanomotors. The pH in the TME is slightly acidic (pH 6.5–6.8) that decreases to 4.5–5.5 in the endo/lysosomes of tumor cells,[24]

*Institute of Molecules and Materials, Radboud University, Heyendaalseweg 135, 6525 AJ Nijmegen, The Netherlands. E-mail: d.wilson@science.ru.nl*

†Electronic supplementary information (ESI) available: Materials, Experimental section, additional figures for MSD curves and fluorescence imaging. See DOI: 10.1039/d0nr04415f

due to the Warburg effect, *i.e.*, metabolism through glycolysis that produces lactate.[25] Gao *et al.* fabricated pH-responsive biocatalytic micromotors by the super-assembly of catalase and succinylated β-lactoglobulin that propel in the presence of $H_2O_2$ and release DOX upon endocytosis and particle degradation in cellular acidic compartments. The mechanism is based on reversible gelation of succinylated β-lactoglobulin depending on pH conditions. Even though the system was successful in showcasing the proof-of-concept study for exploiting physiological conditions, $H_2O_2$ was supplemented externally to cell culture.[26] In another example, Janus nanoparticles comprising hydroxyapatite were fabricated with urease and hyaluronic acid that facilitated tumor penetration due to active motion, thus enhancing uptake by tumor cells. Upon delivery into tumor cells, the increasing solubility of hydroxyapatite helped in the controlled release of drugs to tumor cells.[24] Also, tadpole-like structures with size less than 100 nm with functionalized catalase were fabricated to propel in the presence of $H_2O_2$ in the TME.[27] Even though motion was achieved in both systems, the fuel required for propulsion was supplied externally and was not endogenously produced by the tumor microenvironment. Another major drawback was functionalization of enzymes on the outside of the nanomotors that can be deactivated in the TME. Inorganic nanoparticles such as calcium carbonate ($CaCO_3$), known to dissolve under acidic conditions,[28] are biocompatible and can be used for pH-responsive cancer therapy. Until now, they have been widely used for passive delivery of drugs that can be anchored onto $CaCO_3$ particles by co-precipitation, and once they are in the vicinity of tumor cells, they release the drugs due to low pH conditions and cause cell death.[29] Sen *et al.* showed the release of $Ca^{2+}$, $HCO_3^-$, $OH^+$ and $H^+$ ions upon dissolution of $CaCO_3$ to induce particle movement. The mechanism is based on the diffusioosmosis process created by the difference in diffusion coefficients of the generated ions,[30] which could be utilized to power much smaller motors in the nanometer range under weak acidic conditions.[31] We envisioned that $CaCO_3$ nanoparticles could be used to achieve active motion of our stomatocyte nanomotors in the slightly acidic environment present in the TME as potential DDS for biomedical applications. Our group pioneered the fabrication of supramolecular assemblies by a "bottom-up approach" called stomatocytes,[32] which are made up of amphiphilic di-block copolymers providing a soft interface to the cells and thus can be utilized for delivery of drug molecules.[19] Herein, for the first time, we fabricated nanomotors by growing *in-situ* $CaCO_3$ nanoparticles inside supramolecular architectures which play the role of a nanoreactor and studied their motion behavior in the presence of HeLa cells to simulate the TME. The smart nanomotors were observed to be activated under slightly acidic pH conditions and were able to propel autonomously towards HeLa cells, as a truly "pH tactic" system. Furthermore, DOX molecules were loaded into $CaCO_3$ stomatocytes ($CaCO_3$-sto) structures by co-precipitation and the hybrid motile system was used for actively delivering into HeLa cells. This approach avoids the use of complicated functionalization for active delivery of cargoes in the biological environment and also the use of an external fuel source to power nanomotors, which opens up opportunities for new applications under *in-vivo* conditions.

## Results and discussion

The schematic for the facile approach used to grow "*in-situ*" $CaCO_3$ nanoparticles in the stomach of stomatocytes for having autonomous motion under weak acidic conditions is shown in Fig. 1. In order to avoid any complicated methods for $CaCO_3$ nanoparticle formation, we focused on a well-known, simple and easy precipitation reaction between $CaCO_3$ and $Na_2CO_3$.[33]

Briefly, the $CaCl_2$ salt was initially encapsulated in the stomach during the shape transformation of polymersomes into stomatocytes by dialyzing the polymersomes with an aqueous solution of $CaCl_2$ followed by dropwise addition of $Na_2CO_3$ solution and stirring overnight at 500 rpm. During the procedure, $Na_2CO_3$ solution can pass through the opening of stomatocytes to react with $CaCl_2$ and form $CaCO_3$ nanoparticles by a precipitation reaction. The as-formed stomatocytes were studied by TEM that indicated the presence of the $CaCl_2$ salt as a dark region (Fig. 2b) before $Na_2CO_3$ addition and a porous structure formation in the stomach (Fig. 2c) after $Na_2CO_3$ addition due to the formation of $CaCO_3$ nanoparticles. A well-defined opening was also observed by cryo-TEM (Fig. 2d), which is important for the decomposition of $CaCO_3$ nanoparticles under acidic pH conditions, which further leads to powering the nanomotors. From DLS measurements, the sizes of empty and $CaCl_2$ stomatocytes were observed to be around 340 nm and 376 nm for *in-situ* formed $CaCO_3$-sto (Fig. 2e). It is noteworthy that $CaCO_3$ was in the nanosize

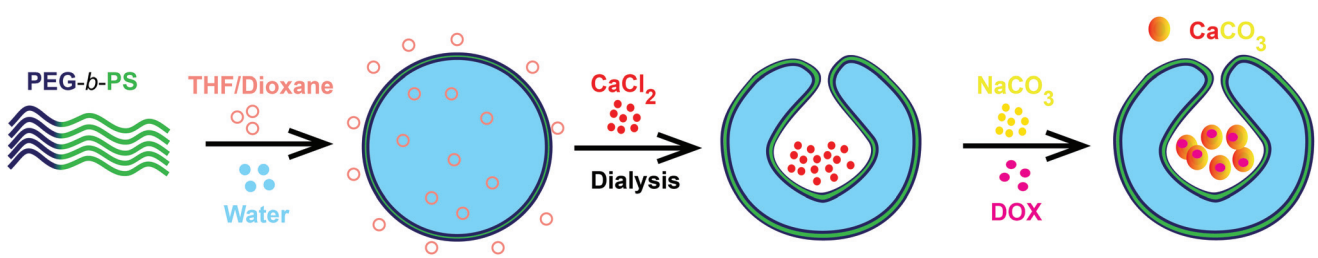


Fig. 1 Schematic representation of the *in-situ* formation of $CaCO_3$ nanoparticles in stomatocytes.

 

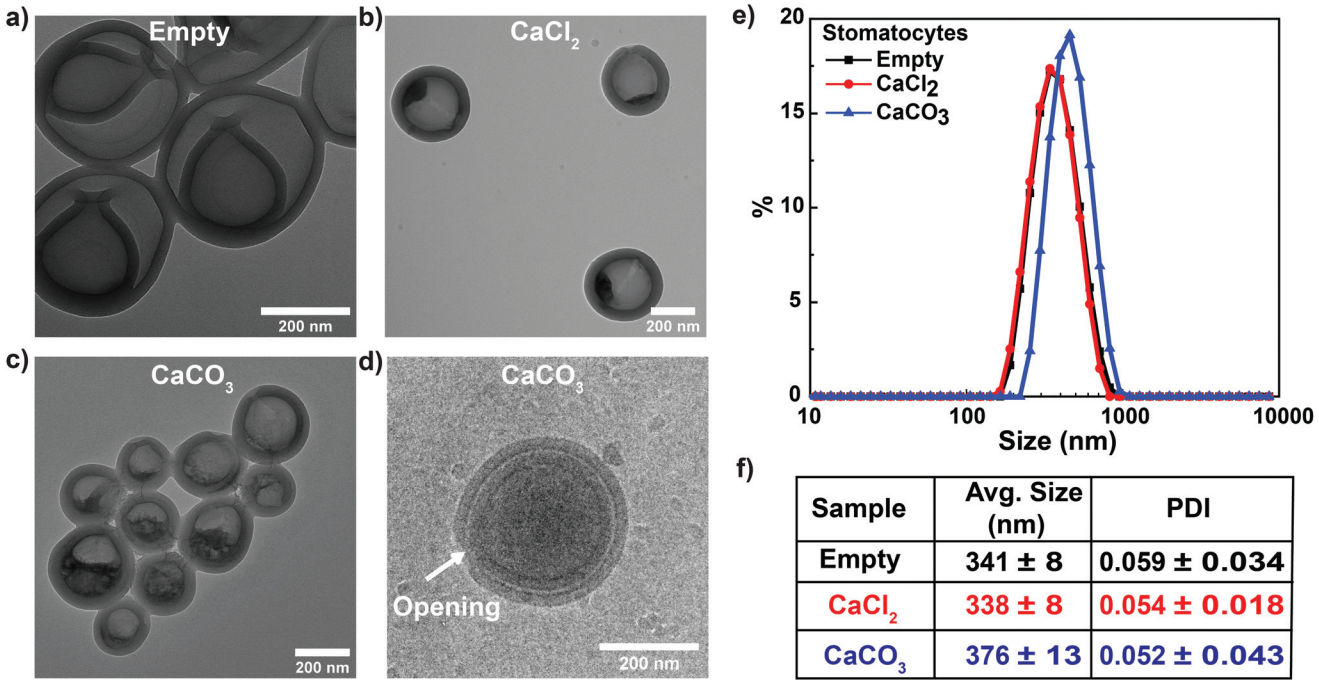


| Sample | Avg. Size (nm) | PDI |
|---|---|---|
| Empty | 341 ± 8 | 0.059 ± 0.034 |
| $CaCl_2$ | 338 ± 8 | 0.054 ± 0.018 |
| $CaCO_3$ | 376 ± 13 | 0.052 ± 0.043 |

**Fig. 2** Structural characterization of stomatocytes. TEM images of (a) empty, (b) $CaCl_2$ and (c) $CaCO_3$ stomatocytes and (d) the cryo-TEM image showing the opening of the stomatocytes. (e and f) DLS measurements of empty, $CaCl_2$ and $CaCO_3$ stomatocytes showed a size of around 341, 338 and 376 nm, respectively, with a narrow PDI.

regime due to the templating effect from stomatocytes during its formation. Previously, such a technique was reported for metal nanoparticle entrapment in stomatocytes where the stomach had a similar effect on the formation of Pt nanoparticles by controlling and confining the nucleation sites.[34]

In tumor cells, lactic acid is produced as a by-product due to anaerobic glucose metabolism inducing acidosis,[35] with pH values around 6.0–6.5 in the tumor intracellular environment[36] and 4.5–5.5 in the endo/lysosomes[37] of tumor cells. In order to simulate the above acidic conditions induced naturally by HeLa cells, $CaCO_3$-sto were studied for the autonomous motion in buffers of pH 4.6, 6 and 7 using nanoparticle tracking analysis (NTA). The mean-square displacement (MSD) curves were obtained by following trajectories in NTA and fitted by linear fit or parabolic fit for Brownian and propelled motion, respectively. According to the self-diffusiophoretic model proposed by Golestanian and coworkers, the speed of the nanomotors was deduced by the following equation:[38]

$$r^2 = 4D\Delta t + (v\Delta t)^2$$

Under neutral pH conditions, $CaCO_3$-sto showed Brownian motion, and with a decrease in the pH from 6 to 4.6, an increase in the speed was observed from 6.5 to 9 μm $s^{-1}$ (Fig. 3a). In comparison, only Brownian motion was observed for the control $CaCl_2$-sto samples (ESI Fig. S2†) at all pH values, instigating $CaCO_3$ dissolution in slightly acidic pH as the driving force. The motion mechanism behind $CaCO_3$-sto is due to the self-dissolution of $CaCO_3$ nanoparticles inside stomatocytes under acidic conditions to ions such as $Ca^{2+}$, $HCO_3^-$ and $OH^-$. These self-generated ions introduce a chemical gradient around the stomatocytes due to the difference in their diffusion coefficient and cause diffusioosmotic flows[31] powering the stomatocytes. A similar self-diffusiophoresis mechanism has been studied to actuate nanomotors in the presence of glucose using cascade enzymatic reactions involving glucose oxidase and catalase.[39] Previously, pH-mediated propulsion of artificial systems has been studied by fabrication of tubular polyaniline/Zn microrockets powered by acidic conditions with speeds reaching up to 100 bodylengths per s.[40] In another example, silica particles coated with polymer multilayers disintegrating by a change in the pH were observed to have active motion and the self-propulsion was reported to result from a broken symmetry due to the polymer concentration gradient along the surface of swimmers.[41] However, the former system requires highly acidic conditions which are not present in the TME and the transition metal Zn is also known to corrode slowly.[42] The latter system used the pH gradient created by NaOH solution in μ-slides that is not present in the TME. Herein, we overcome these issues by using biocompatible and low-cost $CaCO_3$ that can disintegrate in an acidic environment to self-generate a chemical gradient by release of ions in the pH value regime found in the TME and propel the nanomotors. To the best of our knowledge, this is the first study demonstrating the use of $CaCO_3$ to drive supramolecular assembly-based nanomotors.

In order to push the system towards biomedical applications, it is important to study the motion in the physiologi-

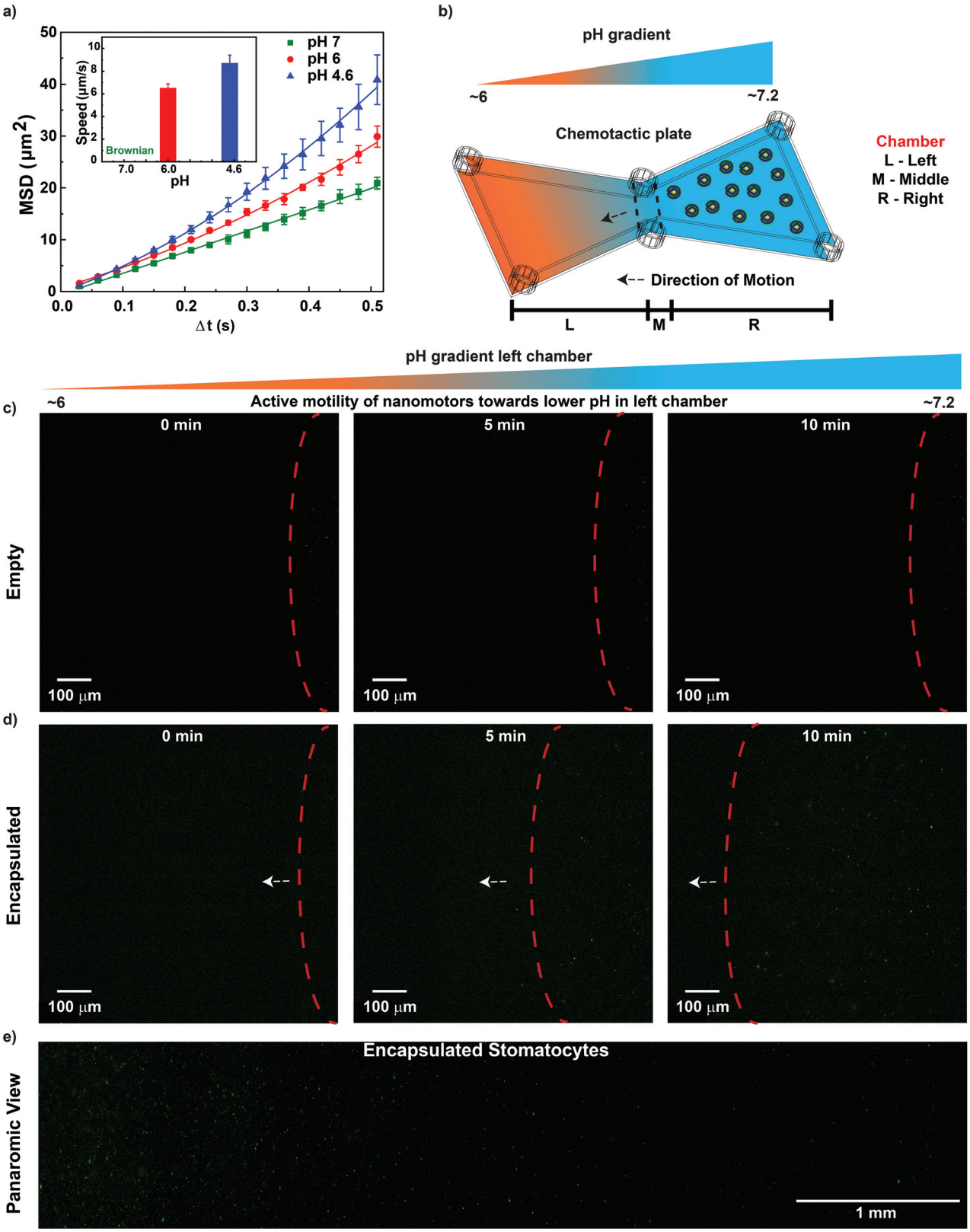


Fig. 3 Motion behavior of $CaCO_3$-sto. (a) MSD curves for $CaCO_3$-sto at pH 4.6, 6 and 7 showcasing propelled motion for the first two and Brownian motion for the latter. An increase in speed was observed with the decrease in the pH. (b) Schematic representation of the chemotactic plate with the established pH gradient. Time lapse fluorescence microscopy images of (c) empty stomatocytes with no directed migration in the pH gradient and (d) $CaCO_3$-sto in the pH gradient showing directed migration towards lower pH conditions. (e) Panoramic view of the left chamber of the chemotactic plate loaded with $CaCO_3$-sto after 1 h showing a larger number of particles in the low pH region.

cally present fuel. Hence, once the autonomous motion of $CaCO_3$-sto was observed, the next step was to extrapolate the system and study its motion behavior in the presence of conditioned tumor cell media that represent the physiologically present fuel. For this purpose, a μ-slide chemotaxis plate from Ibidi was used that contains two chambers on either side separated by a middle chamber that can be used for long-term chemotaxis studies.[43] A schematic representation is shown in Fig. 3b, illustrating the different chambers and the establishment of a pH gradient. The left and middle chambers were filled with conditioned HeLa cell media (pH 6.0); the right chamber was filled with a dilute solution of $CaCO_3$-sto (encapsulated) as the test sample and empty stomatocytes in the case of control experiments. For reliability, all measurements were carried out at the same position in the left chamber of the chemotactic plate. From the chemotaxis experiment, it was observed that $CaCO_3$-sto has directed movement towards lower pH conditions in comparison with Brownian movement for empty stomatocytes. This was witnessed with the increase in the number of particles in the left chamber with increasing time resulting from the migration of $CaCO_3$-sto particles towards lower pH conditions (Fig. 3c and d). The panoramic view of the left chamber of the chemotactic plate (after 1 h) showed an increase in the number of particles with increasing pH gradient that was not observed for empty stomatocytes (ESI Fig. S3†). The control experiments rule out the possibility of the Marangoni effect, drift effects and convection gradients for the movement of $CaCO_3$-sto in the chemotactic plate. Further proof for the migration of particles in the pH gradient was obtained by monitoring the middle and left chambers at 0 and after 30 min (ESI Fig. S4†). In the case of empty stomatocytes, there was no migration observed in both the chambers at the two time points, but for $CaCO_3$-sto, a decrease in the number of particles was observed in the middle chamber and also significant particles were observed to be migrated to the end of the left chamber after 30 min. This showcases the directed motion of $CaCO_3$-sto in the pH gradient generated by HeLa cell cultured media, making it the first truly "pH tactic" supramolecular assembly-based system without the use of any external fuel source/stimuli.

Once the "pH taxis" of the fabricated stomatocytes was observed in the physiologically relevant fuel generated by conditioned HeLa cells, their application for drug delivery was further studied. For this purpose, DOX-loaded $CaCO_3$-sto (DOX/$CaCO_3$-sto) were fabricated and used as DDS towards HeLa cells. Initial studies were conducted for studying the cellular uptake of free DOX or DOX/$CaCO_3$-sto by incubating them with HeLa cells and visualized using confocal laser scanning microscopy (CLSM). After 4 h of incubation, the DOX molecules were observed to be taken up by HeLa cells for both systems and were present in the cell nucleus (Fig. 4a). In the case of free DOX, the cellular uptake was observed to be due to

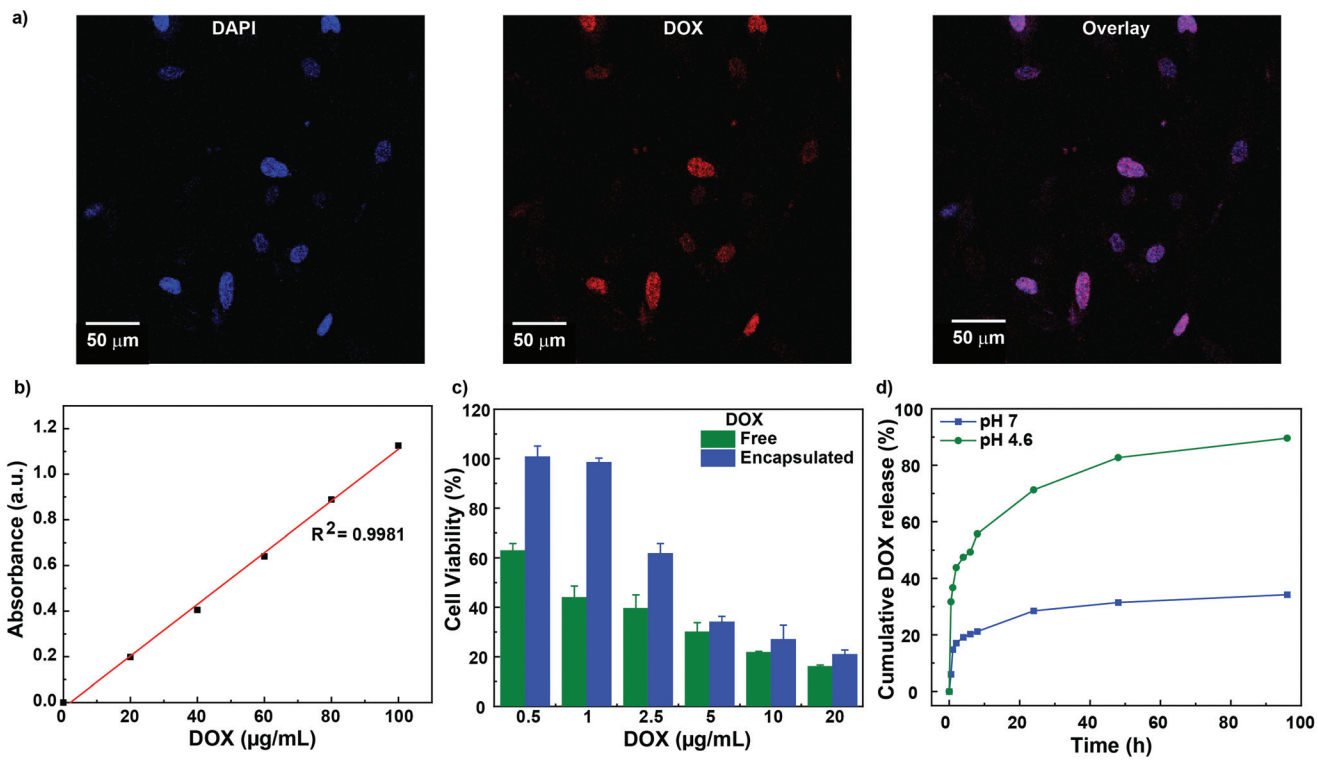


Fig. 4 Drug delivery to HeLa cells by $CaCO_3$-sto. (a) CLSM images of the HeLa cell nucleus stained with DAPI (blue), DOX (red) and an overlay of both after 4 h of incubation. DOX molecules were observed to accumulate in the cell nucleus. (b) Calibration curve for calculating DOX entrapment in $CaCO_3$-sto and (c) cytotoxicity assay by CCK8 for free and entrapped DOX after 48 h of incubation. (d) DOX release assay at basic (pH 7.0) and acidic pH (pH 4.6); increased DOX release was observed at acidic pH.

passive diffusion to the nucleus, whereas for $CaCO_3$-sto-loaded DOX, it was due to the release of the entrapped DOX in the acidic environment of the endosomes.[44] Previously, pH/redox-sensitive DOX-loaded nanoparticles were prepared from poly (ethylene glycol)-block-poly(L-lysine) (PEG-*b*-PLL) for improving cancer therapy and similar results were observed under acidic conditions.[45] However, the system was based on passive delivery. Herein, we expect the use of $CaCO_3$ to both power and actuate stomatocytes to actively target tumor tissues and cells due to the slightly acidic pH, and also for active delivery of drugs due to the ease of entrapment, thereby increasing the bioavailability and efficacy.

Furthermore, cytotoxicity assay was carried out by incubating HeLa cells with free DOX and DOX-entrapped $CaCO_3$-sto to study the *in-vitro* efficacy. First, a calibration curve was obtained for free DOX to calculate the entrapment in $CaCO_3$-sto (Fig. 4b, ESI methods†). Once the entrapped amount of DOX was calculated, equivalent amounts of free DOX and DOX/$CaCO_3$-sto were used for cytotoxicity assays. Free DOX showed higher toxicity in lower concentrations in killing cancer cells, since it can easily diffuse into cells as a molecule in comparison with the entrapped DOX, which must enter cells by endocytosis and be released through endosomes in *in-vitro* experiments (Fig. 4c). However, with the increase of the DOX concentration, DOX/$CaCO_3$-sto had a similar toxicity trend to the free DOX, since the problem encountered for entering the membrane at lower concentrations is overcome, and higher DOX/$CaCO_3$-sto accumulation in cells leads to a high release of DOX. Previously, we have successfully shown cellular uptake of our stomatocyte system to act as delivery agents for tumor cells.[46] Moreover, DOX/$CaCO_3$-sto also has a big advantage as a targeted delivery tool in the biological system, as the motors can be actuated at low pH in the TME by dissolution of $CaCO_3$ invoking pH taxis behavior towards tumor cells and hence the DOX release would take place. This behavior gives rise to active targeted therapy that is expected to be more effective than passive therapy. Also, the dissolution of $CaCO_3$ can result in a pH increase in the TME and inhibit tumor growth,[28] thereby providing an added advantage. In addition, our DDS can escape the mononuclear phagocytic system (MPS) at the blood barrier[47] and enhance the cellular availability of DOX by releasing them without disrupting the membrane of polymersomes since they are entrapped in the stomach of the stomatocyte instead of the lumen of the polymersome membrane as reported in our previous studies.[19] It is also possible that some DOX molecules interact with PEG moieties of the stomatocyte structure and bind to them, which can cause cell death, even after repeated washing steps. However, the main focus of this study was to power nanomotors by encapsulating with $CaCO_3$ and to demonstrate them as a truly "pH tactic" system that can propel by an endogenously produced pH gradient in the TME and as a model example to showcase their capabilities in drug delivery to tumor cells.

In order to prove our methodology that DOX release takes place only at acidic pH due to dissolution of $CaCO_3$, we carried out DOX release experiments at basic (pH 7.0) and acidic pH (pH 4.6) for 96 hours. As anticipated, only at acidic pH, an increase in DOX release was observed up to 90% and was very low under basic pH conditions (Fig. 4d). In the initial period, some DOX release was observed even at basic pH that may be due to leaching of drug molecules from the $CaCO_3$ surface. However, at later stages, only under acidic conditions, the release phenomenon was observed as anticipated, thus showcasing our system to be applicable for controlled drug release in the tumor microenvironment where the pH is close to 4.6.

## Conclusions

We have fabricated active DDS with biocompatible $CaCO_3$-loaded stomatocytes that power motion under slightly acidic conditions provided by the TME. $CaCO_3$-sto were not only observed to show "pH tactic" directional control and movement in the presence of conditioned HeLa cell culture media but could also be used for delivering drug molecules to HeLa cells under *in-vitro* conditions. We believe, under *in-vivo* conditions, our system will have higher efficacy in comparison with free DOX with increased bioavailability at the target site due to its active motion. This fabricated system showcases a facile method to power micro/nanomotors in the endogenously produced physiologically relevant fuel and can substantiate further as active DDS. We envision such a system to be highly beneficial for biomedical applications and can be further extrapolated for the development of fully biodegradable systems with the use of polymers that can degrade under physiological conditions.

## Conflicts of interest

There are no conflicts to declare.

## Acknowledgements

M.M. would like to acknowledge funding from the European Union's Horizon 2020 framework programme under the Marie Skłodowska-Curie Individual Fellowships Grant Agreement No. 794657. D.A.W. and J.S. acknowledge support from the Ministry of Education, Culture and Science (Gravity Program 024.001.035). The authors would like to thank I. Alexopoulos from General Instruments at Radboud University for assistance with confocal images.

## References

1 J. Li, B. E.-F. de Ávila, W. Gao, L. Zhang and J. Wang, *Sci. Rob.*, 2017, **2**, eaam6431.
2 B. E.-F. de Ávila, A. Martín, F. Soto, M. A. Lopez-Ramirez, S. Campuzano, G. M. Vásquez-Machado, W. Gao, L. Zhang and J. Wang, *ACS Nano*, 2015, **9**, 6756–6764.

 

3 O. Felfoul, M. Mohammadi, S. Taherkhani, D. de Lanauze, Y. Zhong Xu, D. Loghin, S. Essa, S. Jancik, D. Houle, M. Lafleur, L. Gaboury, M. Tabrizian, N. Kaou, M. Atkin, T. Vuong, G. Batist, N. Beauchemin, D. Radzioch and S. Martel, *Nat. Nanotechnol.*, 2016, **11**, 941–947.
4 G. Chatzipirpiridis, O. Ergeneman, J. Pokki, F. Ullrich, S. Fusco, J. A. Ortega, K. M. Sivaraman, B. J. Nelson and S. Pané, *Adv. Healthcare Mater.*, 2015, **4**, 209–214.
5 A. Ghosh and P. Fischer, *Nano Lett.*, 2009, **9**, 2243–2245.
6 F. Peng, Y. Tu, Y. Men, J. C. van Hest and D. A. Wilson, *Adv. Mater.*, 2017, **29**, 1604996.
7 Y. Liu, D. Ge, J. Cong, H. G. Piao, X. Huang, Y. Xu, G. Lu, L. Pan and M. Liu, *Small*, 2018, **14**, 1704546.
8 K. Kim, X. Xu, J. Guo and D. Fan, *Nat. Commun.*, 2014, **5**, 1–9.
9 A. M. Boymelgreen, T. Balli, T. Miloh and G. Yossifon, *Nat. Commun.*, 2018, **9**, 1–8.
10 J. Wang, Z. Xiong, X. Zhan, B. Dai, J. Zheng, J. Liu and J. Tang, *Adv. Mater.*, 2017, **29**, 1701451.
11 M. Xuan, Z. Wu, J. Shao, L. Dai, T. Si and Q. He, *J. Am. Chem. Soc.*, 2016, **138**, 6492–6497.
12 C. Chen, F. Mou, L. Xu, S. Wang, J. Guan, Z. Feng, Q. Wang, L. Kong, W. Li, J. Wang and Q. Zhang, *Adv. Mater.*, 2017, **29**, 1603374.
13 B. Dai, J. Wang, Z. Xiong, X. Zhan, W. Dai, C.-C. Li, S.-P. Feng and J. Tang, *Nat. Nanotechnol.*, 2016, **11**, 1087–1092.
14 W.-P. Li, C.-H. Su, Y.-C. Chang, Y.-J. Lin and C.-S. Yeh, *ACS Nano*, 2016, **10**, 2017–2027.
15 F. Soto, G. L. Wagner, V. Garcia-Gradilla, K. T. Gillespie, D. R. Lakshmipathy, E. Karshalev, C. Angell, Y. Chen and J. Wang, *Nanoscale*, 2016, **8**, 17788–17793.
16 Z. Wu, T. Li, J. Li, W. Gao, T. Xu, C. Christianson, W. Gao, M. Galarnyk, Q. He and L. Zhang, *ACS Nano*, 2014, **8**, 12041–12048.
17 D. Wang, C. Gao, W. Wang, M. Sun, B. Guo, H. Xie and Q. He, *ACS Nano*, 2018, **12**, 10212–10220.
18 F. Peng, Y. Tu, J. C. van Hest and D. A. Wilson, *Angew. Chem., Int. Ed.*, 2015, **54**, 11662–11665.
19 Y. Tu, F. Peng, A. A. M. André, Y. Men, M. Srinivas and D. A. Wilson, *ACS Nano*, 2017, **11**, 1957–1963.
20 V. Garcia-Gradilla, S. Sattayasamitsathit, F. Soto, F. Kuralay, C. Yardımcı, D. Wiitala, M. Galarnyk and J. Wang, *Small*, 2014, **10**, 4154–4159.
21 M. Xuan, J. Shao, X. Lin, L. Dai and Q. He, *Chemphyschem*, 2014, **15**, 2255–2260.
22 X. Ma, A. Jannasch, U.-R. Albrecht, K. Hahn, A. Miguel-López, E. Schäffer and S. Sánchez, *Nano Lett.*, 2015, **15**, 7043–7050.
23 C. Ding, L. Tong, J. Feng and J. Fu, *Molecules*, 2016, **21**, 1715.
24 Z. Chen, T. Xia, Z. Zhang, S. Xie, T. Wang and X. Li, *Chem. Eng. J.*, 2019, **375**, 122109.
25 H. Wu, Z. Ding, D. Hu, F. Sun, C. Dai, J. Xie and X. Hu, *J. Pathol.*, 2012, **227**, 189–199.
26 S. Gao, J. Hou, J. Zeng, J. J. Richardson, Z. Gu, X. Gao, D. Li, M. Gao, D. W. Wang and P. Chen, *Adv. Funct. Mater.*, 2019, **29**, 1808900.
27 H. Li, Z. Sun, S. Jiang, X. Lai, A. Böckler, H. Huang, F. Peng, L. Liu and Y. Chen, *Nano Lett.*, 2019, **19**, 8749–8757.
28 A. Som, R. Raliya, L. Tian, W. Akers, J. E. Ippolito, S. Singamaneni, P. Biswas and S. Achilefu, *Nanoscale*, 2016, **8**, 12639–12647.
29 Z. Dong, L. Feng, W. Zhu, X. Sun, M. Gao, H. Zhao, Y. Chao and Z. Liu, *Biomaterials*, 2016, **110**, 60–70.
30 J. J. McDermott, A. Kar, M. Daher, S. Klara, G. Wang, A. Sen and D. Velegol, *Langmuir*, 2012, **28**, 15491–15497.
31 M. Guix, A. K. Meyer, B. Koch and O. G. Schmidt, *Sci. Rep.*, 2016, **6**, 1–7.
32 I. Ortiz-Rivera, M. Mathesh and D. A. Wilson, *Acc. Chem. Res.*, 2018, **51**, 1891–1900.
33 Y. Ueno, H. Futagawa, Y. Takagi, A. Ueno and Y. Mizushima, *J. Controlled Release*, 2005, **103**, 93–98.
34 D. A. Wilson, R. J. M. Nolte and J. C. M. van Hest, *J. Am. Chem. Soc.*, 2012, **134**, 9894–9897.
35 L. E. Gerweck and K. Seetharaman, *Cancer Res.*, 1996, **56**, 1194–1198.
36 F. A. Gallagher, M. I. Kettunen, S. E. Day, D.-E. Hu, J. H. Ardenkjær-Larsen, R. i. t. Zandt, P. R. Jensen, M. Karlsson, K. Golman, M. H. Lerche and K. M. Brindle, *Nature*, 2008, **453**, 940–943.
37 C.-Y. Sun, Y. Liu, J.-Z. Du, Z.-T. Cao, C.-F. Xu and J. Wang, *Angew. Chem., Int. Ed.*, 2016, **55**, 1010–1014.
38 R. Golestanian, T. B. Liverpool and A. Ajdari, *Phys. Rev. Lett.*, 2005, **94**, 220801.
39 P. Schattling, B. Thingholm and B. Städler, *Chem. Mater.*, 2015, **27**, 7412–7418.
40 W. Gao, A. Uygun and J. Wang, *J. Am. Chem. Soc.*, 2012, **134**, 897–900.
41 M. Fernández-Medina, X. Qian, O. Hovorka and B. Städler, *Nanoscale*, 2019, **11**, 733–741.
42 L. Yin, H. Cheng, S. Mao, R. Haasch, Y. Liu, X. Xie, S.-W. Hwang, H. Jain, S.-K. Kang, Y. Su, R. Li, Y. Huang and J. A. Rogers, *Adv. Funct. Mater.*, 2014, **24**, 645–658.
43 P. Zengel, A. Nguyen-Hoang, C. Schildhammer, R. Zantl, V. Kahl and E. Horn, *BMC Cell Biol.*, 2011, **12**, 21.
44 A. Helenius, I. Mellman, D. Wall and A. Hubbard, *Trends Biochem. Sci.*, 1983, **8**, 245–250.
45 G. Zhang, Y. Zhu, Y. Wang, D. Wei, Y. Wu, L. Zheng, H. Bai, H. Xiao and Z. Zhang, *RSC Adv.*, 2019, **9**, 20513–20517.
46 J. Sun, M. Mathesh, W. Li and D. A. Wilson, *ACS Nano*, 2019, **13**, 10191–10200.
47 M. A. Dobrovolskaia and S. E. McNeil, *Nat. Nanotechnol.*, 2007, **2**, 469.